J. Phys. B: At. Mol. Opt. Phys. **42** (2009) 044014 (7pp) doi:10.1088/0953-4075/42/4/044014

Multiphoton adiabatic rapid passage: classical transition induced by separatrix crossing

Türker Topçu and F Robicheaux

Department of Physics, Auburn University, AL 36849-5311, USA

Received 17 October 2008, in final form 18 November 2008
Published 3 February 2009
Online at stacks.iop.org/JPhysB/42/044014

Abstract

A recent experiment showed that significant population transfer for a ∼10 photon resonance could be obtained with a relatively small chirp in the light field. The system investigated was the microwave transition between Rydberg states in Li from $n = 72$, $\ell = 1$ to $n \sim 82$. This is a multiphoton resonance in a one-electron system. We present quantum calculations using a model one-dimensional system and a fully three-dimensional system that agree with the measured results and the original interpretation of the transition as an adiabatic passage through a multiphoton resonance. Although the measured results strongly suggest a simple multiphoton transition, the quantum calculations clearly indicate that more than 50 photons are absorbed/emitted in this process. We also performed classical calculations for this system and found that the classical transitions also give a small energy band near the multiphoton resonance. However, the interpretation of the results is quite different and is an example of transitions induced by separatrix crossing. The separatrix arises from the classical resonance between the microwave frequency and the classical Rydberg frequency at an energy between the initial and final states.

1. Introduction

The multiphoton transition between states separated by several quanta has been studied in many systems. A useful method for controlling the transitions is to chirp the frequency of the photons so that a series of transitions takes place. This is sometimes called ladder climbing. For example, [1] caused the transition from the ground vibrational state of NO to the $v = 3$ state by chirping an IR pulse through the transitions $v = 0 \rightarrow 1$ then $v = 1 \rightarrow 2$ and then $v = 2 \rightarrow 3$. Another example is [2] which used a chirped microwave pulse to change the principal quantum number, n, of an atomic Rydberg state. (See the first paragraph of [3] for other examples.)

Although the systems are quantized, there is a simple classical interpretation of these results. The light field makes a stable island in phase space for parameters where the classical unperturbed frequency of the system matches the frequency of the light field. When a potential is not perfectly harmonic, the frequency of the unperturbed system depends on energy; thus, the energy of the system can be controlled by changing the frequency of the light. As an example, suppose an atom in the $n = 72$ state is exposed to a light field whose frequency exactly matches the classical Rydberg frequency. There is a finite probability that the electron is captured into the stable island that is formed near $n = 72$. (Essentially, the electron gets phase-locked to the light.) Now, if the frequency is decreased adiabatically, the island will move to higher n and the electron, still trapped in the island, will decrease in binding energy. By controlling the size and direction of the chirp, the final energy of this classical system can be controlled.

As pointed out in [3], the chirp needed to make a transition over many quantum numbers could be substantial. In the example they chose, one would need to chirp the frequency from roughly 17.3 to 12.2 GHz to go from $n = 72$ to $n = 82$ through ladder climbing. In order to avoid this very large chirp, they suggested a direct 10-photon transition but with a much smaller chirp (roughly 500 MHz compared to 5 GHz) that goes from low to high frequency. Since the transition is not single-photon resonant, a larger field strength is needed for the transition. The results of their measurement clearly demonstrated this effect as they were able to cause transitions from the Li $n = 72, \ell = 1$ state to states near $n = 82$ with roughly 80% efficiency. This was accomplished with a small chirp, but an appealing feature of this method was that

the size of the effect did not strongly depend on the size of the chirp. They interpreted their results using a qualitative quantum picture involving a multiphoton resonance.

An important aspect of this process is the relative frequencies involved. The transition frequency to go directly from $n = 72$ to 82 using ten identical photons is 14.5 GHz[1]. Thus, the driving frequency is red detuned by roughly 2.8 GHz for single-photon transitions near $n = 72$ and is blue detuned by roughly 2.3 GHz for single-photon transitions near $n = 82$. Thus, the microwaves are strongly detuned from single-photon transitions out of the initial state and into the final state. The frequency 14.5 GHz exactly matches the classical Rydberg frequency for $n = 76.8$ which is roughly half-way between the initial and final states.

In this paper, we present the results of fully quantum calculations for this system. We numerically solve the time-dependent Schrödinger equation for a one-dimensional model and for a full three-dimensional calculation for Li using a model potential that gives the correct quantum defects of the Rydberg states. We are able to confirm that the results of the measurement are due to the microwave transitions described in [3]. We also performed three-dimensional quantum calculations for H and found substantial (quantitative) differences with the Li results due to the non-zero quantum defects of the $\ell = 0$ and $\ell = 1$ states of Li. Also, we found that an off-diagonal ac Stark shift substantially contributes to the ℓ-mixing in the quantum calculations. Actually, we found substantial ℓ-mixing well beyond the values that would be expected from a 10-photon transition. Thus, the interpretation in [3] as a 10-photon transition needs to be modified; the calculations clearly show that at least 50 photons are absorbed/emitted during the transition. It is more appropriate to say that the transition occurs by chirping through a 10-photon resonance condition.

We also performed classical calculations for this system. To our great surprise, we found that the classical system also evolved from a specific initial state to a small band of final energies even though there is no obvious classical resonance near the starting and final energy. We traced this classical result to the change of an adiabatic invariant due to a separatrix crossing [4, 5]. The procedure uses the adiabatic change of a variable in the Hamiltonian to cause orbits with a particular value of an adiabatic invariant to cross a separatrix and jump to a different value of the invariant; the size of the jump depends on the properties of the Hamiltonian. The trajectory in phase space evolves from one edge of the chaotic region to another edge through a fully chaotic region. If the initial distribution is localized to a small range of the adiabatic invariant, then this slow evolution of the Hamiltonian can cause transitions with a high degree of final state specificity. In [6], they slowly increased and then decreased the strength of an IR field for a driven Morse oscillator; they found that the final population was localized to a small range near the initial and target vibrational energy (see their figure 4).

[1] In [3], they used a frequency of 15.2 GHz which is clearly different from the 10-photon resonant value. The experimental frequency of 15.2 GHz is more nearly an 8-photon transition to $n = 80$, and this is probably the actual final states that were produced.

In section 2, we present the results of our three-dimensional quantum calculations. We show that the chirped pulse can cause transitions to particular final states, describe the role that the ac Stark effect plays in the ℓ-mixing, and contrast the transition in Li with that in H. In section 3, we present the results of a one-dimensional model calculation. As this is a quantitative version of the model presented in [3], the results show that their simple model does give similar behaviour although it clearly does not include the large amount of ℓ-mixing in the full three-dimensional system. In section 4, we present the results of classical one-dimensional and three-dimensional results. We show that the classical system has a similar specificity in the final state as the quantum system, present the results from a time-dependent analysis using the Poincare surface of section map, and give an interpretation of the mechanism for the transition based on the jump in the value of an adiabatic invariant due to separatrix crossing [4, 5].

Atomic units are used unless SI units are specifically given.

2. Quantum calculation: three dimensions

The time-dependent calculations were performed in the manner described in [7] but with the magnetic field set to 0 and the electric field $\mathcal{F}$ having the time dependence of a chirped microwave field. The other difference is that [7] solved for an inhomogeneous Schrödinger equation where there is a source term, S_0. For this paper, there is no source term so $S_0 = 0$. The main features of the method are described below; the reader is directed to [7] for a more detailed treatment of the numerical method.

The wavefunction is represented as the superposition of radial functions times spherical harmonics:

$$\Psi(r, \theta, \phi, t) = \sum_{\ell} f_{\ell}(r, t) Y_{\ell m}(\theta, \phi), \tag{1}$$

where the time-dependent functions $f_{\ell}(r, t)$ are on a grid of radial points where the radial grid is a square root mesh with the jth point given by $r_j = r_1 j^2$ to efficiently represent the Rydberg states. The propagation of Ψ from t to $t + \delta t$ is performed using an $O(\delta t^3)$ implicit algorithm. The Hamiltonian is split into the atomic Hamiltonian plus the field Hamiltonian, $\mathcal{F}(t) r \cos\theta$, and the contribution of each is included through an $O(\delta t^3)$ split operator method. Because an implicit method is used, the time step can be substantial and is typically 1/500 times the Rydberg period.

Even with this efficiency the calculations are quite time consuming due to the long time range involved: the calculation must cover a time range of roughly 300 ns whereas the Rydberg period for $n = 72$ is roughly 60 ps. Thus, the time range is over 5000 Rydberg periods, and we use 500 time steps per period for over two million time steps for each set of parameters (atom type, field strength, etc). The calculations were performed on a local pc or unix workstation.

The convergence of the calculation was ensured by performing several calculations for the same parameters and varying the time step (δt), the spacing of the radial grid (r_1),

and the radial size of the region contained in the calculation (number of radial mesh points). The convergence with respect to the number of spherical harmonics in the calculation was ensured by taking ℓ_{max} to be $\ell_{tiny} + 10$ where ℓ_{tiny} is the angular momentum that contains less than 10^{-16} of the probability of the wavefunction. Thus, the ℓ_{max} changes with time so that the wavefunction is properly represented but the computation runs faster than for a fixed ℓ_{max}.

In the calculations, the potential for H was taken to be $V = -1/r$. The potential for Li was taken to be a model potential that gives the Li quantum defects for the Rydberg states. The form of the potential for Li is

$$V = -\frac{1 + 2\,e^{-\alpha_1 r} + r\alpha_2\,e^{-\alpha_3 r}}{r} - \frac{\alpha}{2r^4}[1 - \exp(-r^3)]^2 \quad (2)$$

with the parameters $\alpha_1 = 2.8917$ for $\ell = 0$ and 2.8964 for all other ℓ, $\alpha_2 = 0.9476$ for $\ell = 0$ and 3.2052 for all other ℓ, $\alpha_3 = 1.9664$ for $\ell = 0$ and 4.7130 for all other ℓ, and $\alpha = 0.189$. For the radial grids used in the calculation, the numerical quantum defects differed from the actual quantum defects by less than 0.001. The quantum defects are all 0's for H, and for Li are 0.40 for $\ell = 0$, 0.048 for $\ell = 1$ and less than 0.003 for all other ℓ.

In all of the calculations, we chose the form of the electric field to be the same and to closely match that used in the experiment. The form of the electric field was

$$\mathcal{F}(t) = F_{MW} \exp\left(-\left[\frac{t}{\Delta t}\right]^2\right) \cos(\omega t + \dot{w} t^2/2), \quad (3)$$

where F_{MW} is the maximum electric field for the microwaves, Δt is 1/2 the $1/e$ full width of the microwave field, ω is the central microwave frequency, and $\dot{\omega}$ is the microwave chirp. Unless specifically stated otherwise, the width $\Delta t = 50$ ns$/(2\sqrt{\ln 2})$ gives a FWHM of 50 ns and the chirp $\dot{w} = 2\pi 12$ MHz ns^{-2}. These parameters give a chirp of 600 MHz over the FWHM of the microwave field. In the calculations we varied the strength of the microwave field, F_{MW}, and the central frequency, ω, depending on the states involved. Unless explicitly stated otherwise, we always choose $\omega = \Delta E/N_{phot}$ where ΔE is the energy difference between the upper and the lower state, and N_{phot} is the number of photons in the resonance condition.

Figure 1 shows the results of two calculations using Li $n = 72, \ell = 1$ as the initial state. This figure shows the probability that the atom finishes in different n states as a function of F_{MW}. For the 6-photon resonance, the atom mostly transitions to the upper state by ~1.3 V cm^{-1} while the 10-photon resonance requires ~2.6 V cm^{-1}; the dependence on field strength is more complicated for the 10-photon resonance, showing apparent quantum beats between different pathways. The 6-photon resonance shows a substantial mixture of $n = 77$ in the final state. For the 10-photon resonance, roughly 91% of the population is in either $n = 72$ or 82 at 2.6 V cm^{-1}. At higher fields, the 10-photon case gives a substantial spread of states. Figure 2 shows the distribution of states at 2.5 and 3.0 V cm^{-1}. It is clear that only a few principal quantum numbers are populated; at 2.5 V cm^{-1}, 92% of the population is in the 72 and 82 states while this drops to 79% at 3.0 V cm^{-1}.

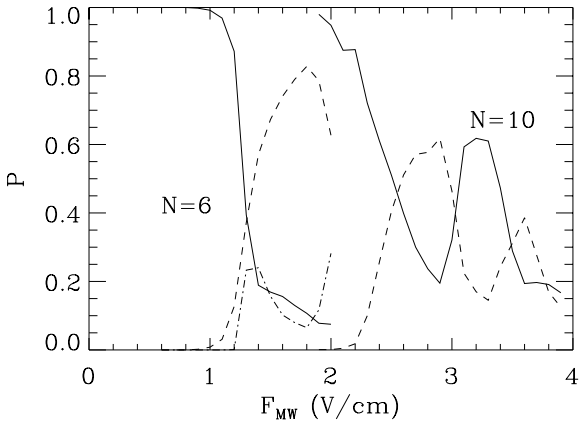

Figure 1. The results of a three-dimensional quantum calculation for the 6-photon resonance condition and the 10-photon resonance condition in Li starting from the 72 p state. As a function of peak microwave field strength, the probability, P, for the state to finish in the $n = 72$ states (the solid line), or the state $72 + N$ (the dashed line) where N is the number of photon resonance. For the 6-photon resonance, there was a substantial amount of transition to the $n = 77$ state (the dash-dot line). To avoid confusion, the data for the $N = 6$ calculations are only shown up to 2.0 V cm^{-1}.

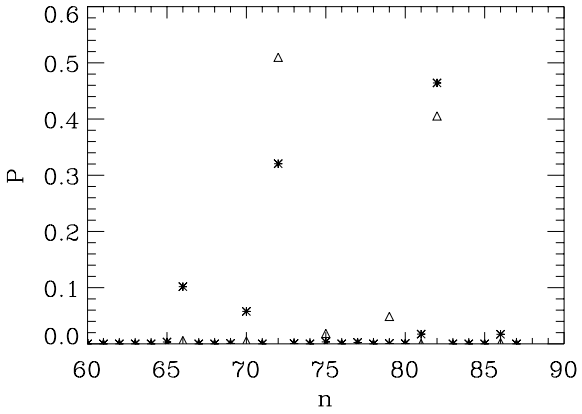

Figure 2. The probability, P, for the state to finish in the n for the 10-photon resonance condition. The triangles are for $F_{MW} =$ 2.5 V cm^{-1} and the asterisks are for 3.0 V cm^{-1}.

From this it is clear that Stark shifts in these high fields are causing different resonance conditions to become important.

Figure 3 shows the data for the 6-photon and 10-photon resonance conditions for H. It is clear that the H atom gives a cleaner population transfer. For example, at 2.5 V cm^{-1} for the 10-photon resonance, more than 99% of the population is in the $n = 72$ or 82 states while this drops to 94% for 3.0 V cm^{-1}. Also, the strong interference pattern in figure 1 is absent for H. This suggests that the reason for the spread in population for Li has to do with the quantum defects. This makes sense because the $\ell = 0$ state of Li is substantially shifted out of the n-manifold and can come into accidental resonance with the microwave photon.

One of the striking features of the calculation was that the probability for the electron to be in a given ℓ was spread over a broad range. For example, figure 4 shows the probability of finding the electron in a particular ℓ summed over all n for the 6-photon resonance from the 72 p state to the $n = 78$ states

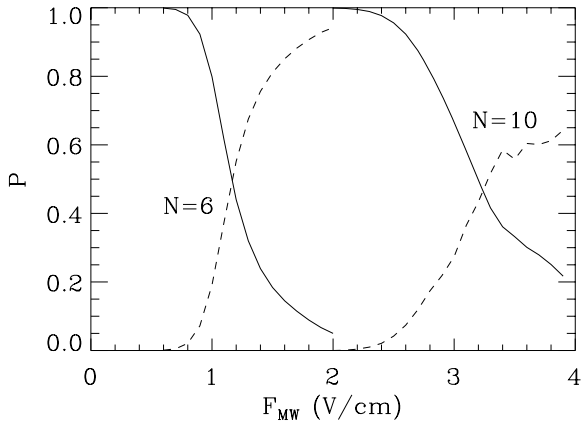

Figure 3. Same as figure 1 but for H.

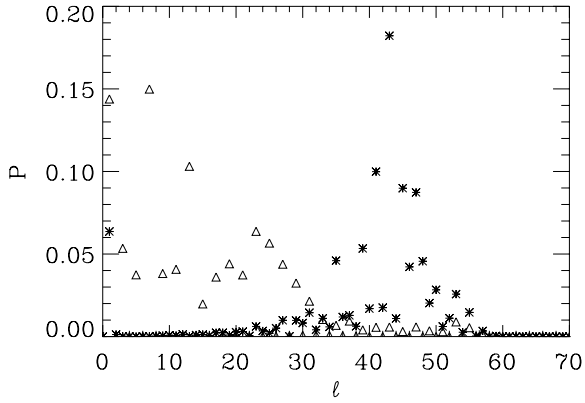

Figure 4. The probability, P, for the state to finish with angular momentum ℓ for the 6-photon resonance condition at a field $F_{\rm MW} = 1.4$ V cm^{-1}. The triangles are for H and the asterisks are for Li. It is not obvious from this graph but the even ℓ are hardly populated for H; one can see only odd ℓ are populated in H by noting that in any $\Delta\ell = 10$ region (e.g. 0–9) only five triangles are visible because they substantially differ from $P \sim 0$.

in H and Li; the field strength is 1.4 V cm^{-1}. At this field strength, Li has 81% transfer into $n = 77$ and 78 while H has 76% transfer into the $n = 78$ states. First, it is completely clear from these distributions that this is not a simple 6-photon resonance since substantial population extends up to $\ell \sim 55$; note that the ℓ population nearly extends up to the maximum allowed for $n = 78$, i.e. $\ell_{\rm max} = n - 1 = 77$. For a 6-photon transition, the ℓ distribution should not extend beyond $\ell = 7$ since each photon can only give $\Delta\ell = \pm 1$. Thus, the indication from figure 1 that this is a relatively straightforward 6-photon transition is an illusion. Although the ℓ distribution suggests that the Li atom absorbs/emits more photons than the H atom, the reverse is the actual case as will be discussed below. Second, the ℓ distributions are qualitatively different for the two atoms. The ℓ population for H is conspicuous in that the even ℓ are hardly populated; the largest probability for an even ℓ is ∼0.001. Another striking feature is that the Li distribution has just over 6% in the $\ell = 1$ states and then less than 1% in any ℓ until $\ell \sim 25$ whereas the H atom has more than 1% population in almost every odd ℓ until $\ell \sim 33$.

The difference in ℓ distribution between H and Li may be somewhat surprising since the Li atom starts in a state with a pretty small quantum defect, 0.048, and in a high principal quantum number. We believe that the difference is due to the coupling between different ℓ that occurs through the ac Stark shift. For the 6-photon resonance condition, the microwave frequency is not resonant with $\delta n = \pm 1$ transitions near $n = 72$ or 78. When the field is weak but not resonant, there are two photon virtual transitions (e.g. $72 \to 73 \to 72$ and $72 \to 71 \to 72$) which lead to an effective Hamiltonian that gives a shift that depends on ℓ and a coupling from ℓ to $\ell \pm 2$. Because all states are degenerate in H, this coupling causes the angular momentum to start changing even in weak fields. However, since Li has a quantum defect for $\ell = 1$, the field needs to become substantial before the coupling is strong enough to cause transition to $n = 72$, $\ell = 3$. Thus, we see the angular distribution in H start to substantially mix well before the peak field but the angular momentum for Li stays in $\ell = 1$ until just before the resonance condition. Once the atoms transition to $n = 78$ the sign of the effective Hamiltonian is reversed from that at $n = 72$; the reason is that ω is less than the Rydberg frequency at $n = 72$ but larger than the Rydberg frequency at $n = 78$. Thus, the angular momenta in H precess in the opposite direction after the transition compared to before the transition which tends to undo a fraction of the high angular momentum components; since Li was restricted to relatively small ℓ until the transition, the ℓ population for Li tends to simply evolve to higher angular momenta after the transition.

3. Quantum calculation: one dimension

We also investigated the behaviour of a one-dimensional model. The large range of angular momenta needed to describe the wavefunction was the reason that the calculations for the full three-dimensional system were time consuming. Also, the wavefunction from a full three-dimensional system can be complicated and difficult to interpret. Finally, [3] interpreted their results using a Floquet calculation of a one-dimensional model. In this picture, the multiphoton transition is the result of an adiabatic crossing between two states connected by a multiphoton resonance condition. For these reasons, we performed a series of calculations where the electron was restricted to one dimension.

We computed the time-dependent wavefunction $\Psi(x, t)$ when the potential is given by $V = -1/x + \mathcal{F}(t)x$ and the range is restricted to $x \geqslant 0$. We used the same parameters for the time-dependent field as in the three-dimensional calculation and started the wavefunction in the $n = 72$ state. Figure 5 shows the population in the final states for the 6-photon and 10-photon resonance conditions as a function of field strength. Although the populations do not exactly behave as for the full three-dimensional calculation, there is a strong similarity to the results in figures 1 and 3. These results show that the one-dimensional model does capture some of the essential physics of this system although the results of section 2 clearly show that the actual system is more nuanced.

Because of the microwave field, it is not obvious when the transition takes place during a run; the microwave field

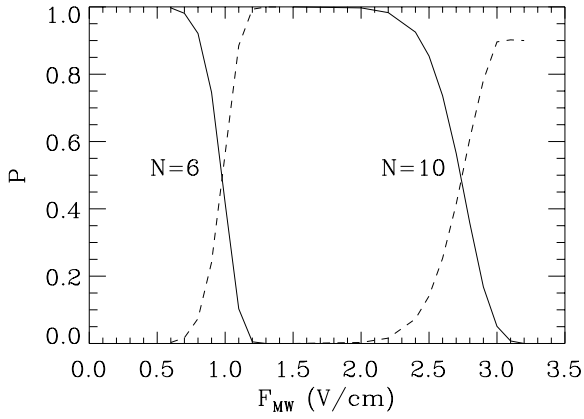

Figure 5. Same as figure 1 but for the one-dimensional model discussed in the text.

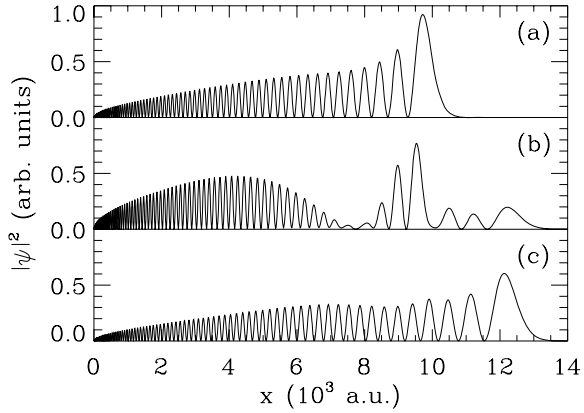

Figure 6. The magnitude of the wavefunction (a) just before, (b) during, and (c) just after the transition. See the text for the detailed times and field strengths.

causes virtual transitions and, thus, the wavefunction in the field is not the zero-field wavefunction. Figure 6 shows $|\Psi|$ as a function of x at three different times: just before, during, and just after the transition. The resonant frequency for the 6-photon transition is 15.65 GHz. The wavefunctions in figure 6 are from a calculation with a peak field strength of 1.2 V cm^{-1} for the 6-photon resonance condition; for this strength, 99.4% of the wavefunction finishes in the $n = 78$ state. The wavefunction in figure 6(a) is at a time of -12.4 ns where the field strength is 1.012 V cm^{-1}, and the frequency is 15.50 GHz. Clearly this wavefunction still appears to be almost completely a single eigenstate even though the projection on the field free $n = 72$ state, $|\langle\Psi|\psi_{72}\rangle|^2$, is roughly 0.47 and the projection on $n = 78$ is less than 0.01. The wavefunction in figure 6(b) is at a time of 0.4 ns where the field strength is 1.200 V cm^{-1} and the frequency is 15.65 GHz; clearly this wavefunction is in the midst of the transition since it does not look like either the initial or the final state. Note that $|\Psi|^2$ is nearly going to 0 at each minimum; although not conclusive, this indicates that the wavefunction roughly has the form $\exp(-i\alpha)y(x)$ where α is a real phase and $y(x)$ is a real function: thus, a single eigenstate of a complicated Hamiltonian. Perhaps more surprising is that the probability to be in the field free $n = 72$ state is 0.11 and to be in the $n = 78$ state is 0.06 which means that most of the wavefunction are neither in the initial nor in the final state. The wavefunction in figure 6(c) is at a time 10.6 ns where the field strength is 1.059 V cm^{-1} and the frequency is 15.77 GHz; although there is a slight ripple on the maxima, this is clearly a wavefunction that is almost completely a single eigenstate even though the projection on the $n = 78$ state is 0.35 and the projection on the $n = 72$ state is less than 0.01.

An important factor about figures 6 is that if the microwave has a peak field strength of 1.0 V cm^{-1} the probability for finishing in the $n = 78$ state is 0.55; this probability increases to 0.88 at a field strength of 1.1 V cm^{-1}. Thus, it is clear that the reason for the transition occurring in figure 6(b) is not because of the slight increase in the field strength but due to the chirp passing through the resonance condition.

4. Classical calculation

There are many reasons that might lead one to expect that a classical simulation of this system would not give results similar to that from a fully quantal calculation. For example, the 6-photon resonance in H from $n = 72$ predominantly gives only population in $n = 72$ and $n = 78$ until the field strength gets very large. It is not at all clear what classical mechanism would give such specificity in the final state. However, the quantum calculations are at high principal quantum numbers and involve many photons, so perhaps some sort of correspondence principle applies. Unlikely as it seems, there is a classical mechanism that will give a final energy distribution that is highly localized just at the right energy. The mechanism is based on the jump in an adiabatic invariant due to a separatrix crossing [4–6].

We performed classical calculations for the 6-photon resonance from $n = 72$. The calculation used 1000 trajectories that were in a micro-canonical distribution at the $n = 72$ energy but only with orbits that start with $1 < L < 2$ and $|L_z| < 1/2$. We used exactly the same microwave field as in the quantum calculation and numerically solved the classical equations of motion to get the final distribution of energy. A trajectory was counted for the state n if its energy after the microwave was turned off was between $-1/[2(n-1/2)^2]$ and $-1/[2(n+1/2)^2]$.

Figure 7 shows the distribution of final n for microwave field strengths of 1.5, 1.7, 2.0 and 2.4 V cm^{-1}. Surprisingly, the final state energy is almost completely in either the $n = 72$ initial state or the 78 final state for fields of 2.0 or less. It is only at the large field, 2.4 V cm^{-1}, that there is a spread in the final states. This is incredibly similar to the behaviour of the quantum calculations. Somehow the classical calculation reproduces a 6-photon resonance. The probability for being in the initial and final states versus the field strength shows a behaviour qualitatively similar to that in the quantum calculation in figure 3.

It is important to note that there are substantial differences between the classical and quantum results. As an example, the quantum 6-photon resonance in the three-dimensional calculation of H gives 50% transition for a field between 1.1 and 1.2 V cm^{-1} whereas the classical field is higher, between

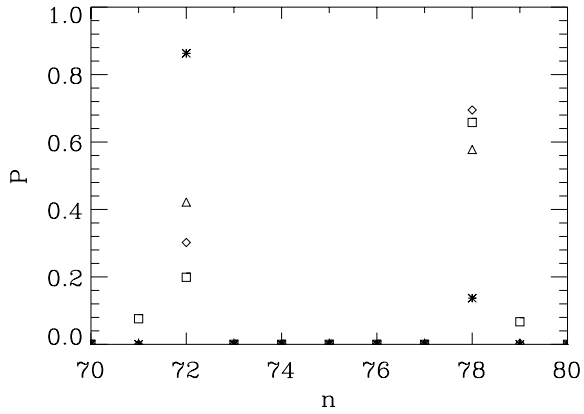

Figure 7. Same as figure 2 but for the 6-photon resonance in the hydrogenic classical model discussed in the text. The asterisks correspond to $F_{\rm MW} = 1.5$ V cm^{-1}, the triangles are for 1.7 V cm^{-1}, the diamonds are for 2.0 V cm^{-1} and the squares are for 2.4 V cm^{-1}.

1.6 and 1.7 V cm^{-1}. This is likely due to the choice of the initial distribution of trajectories. There are substantial discussions in the literature about the best choice of classical initial conditions to reproduce a quantum calculation. Instead of pursuing these details we are more interested in the mechanism that could be causing this high degree of localization in the classical calculation.

In order to trace the classical mechanism that controls the transition, we also performed classical calculations for the one-dimensional model. The model is for a potential which is $-1/x + \mathcal{F}(t)x$ with an infinite wall at $x = 0$. This model showed a similar localization of final states to the $n = 72$ and 78 states, but the calculations with the chirp were hard to interpret. To understand the results, we performed the calculation at a microwave field of 1.47 V cm^{-1} which is a little larger than the field where transitions occur. In figures 8, we show the phase space position of all the trajectories at three different times: just before, during, and just after the transition. To put the positions on the plot, we chose a time where the phase of the microwave field, $\phi = \omega t + \dot{w}t^2/2$, was equal to $2\pi j + \pi/2$ where j is an integer. Taking the energy at that time to be $E = v^2/2 - 1/x$ and a parameter $\beta \equiv -xE$, the y-axis is the action and is given as $I = 1/\sqrt{-2E}$, and the x-axis is the phase of the orbit and is $\theta = 2[\sin^{-1}(\sqrt{\beta}) - \sqrt{\beta(1-\beta)}]$ if $v > 0$ and $\theta = 2\pi - 2[\sin^{-1}(\sqrt{\beta}) - \sqrt{\beta(1-\beta)}]$ if $v < 0$. The points from the chirped microwave calculation are the +'s. Figures 8(a) and (c) are over the same range but figure 8(b) expands the region of phase space near the separatrix.

Note that the +'s tend to lie on simple curves. In order to understand the origin of these curves, we have included (as dots) the result of a Poincaré surface of section (SOS) plot that was generated by using the instantaneous frequency and field strength that correspond to the times in figures 8. There are several conspicuous features of the SOS plot that have been understood for a long time. We will explain figure 8(a). The most obvious feature is the concentric closed lines centred at $I \simeq 75$ and $\theta/2\pi \simeq 0.25$. These arise from the electron locking to the phase of the microwave and is an island of stability. Far above and below the island are points that form lines that do not close but go all the way across;

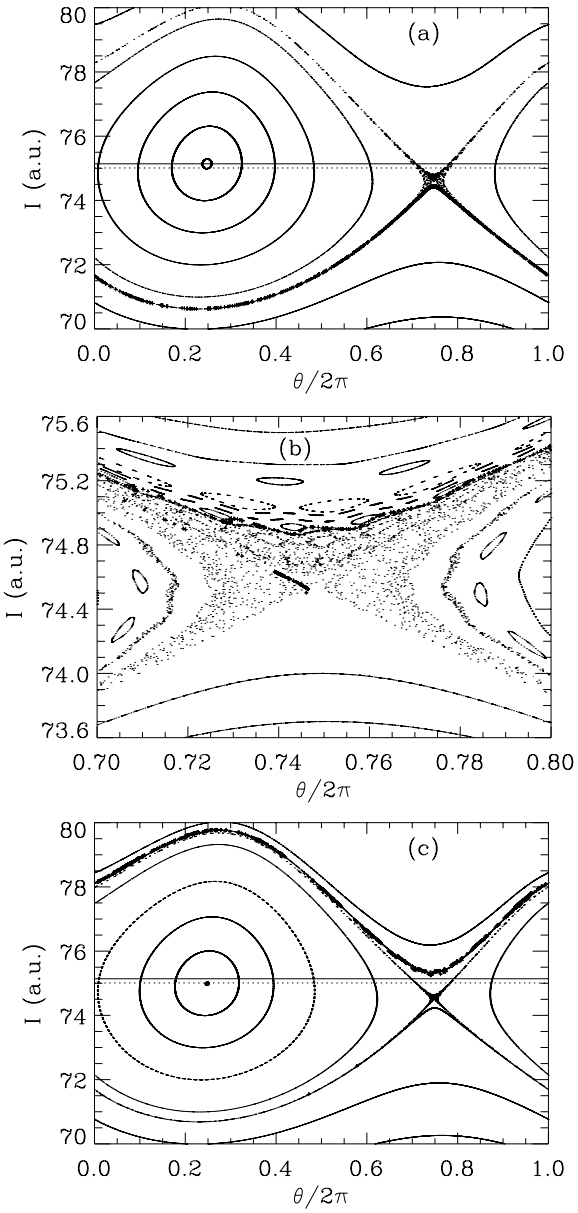

Figure 8. The phase space position of the trajectories at a time (a) just before, (b) during, and (c) just after the transition. These calculations are for a one-dimensional model discussed in the text. The +'s are the actual phase space positions. The small dots (which in some regions are so close together that it appears to be lines) are from a Poincaré surface of a section map that corresponds to the instantaneous field strength and frequency corresponding to each time. The solid horizontal line in (a) and (c) marks the position of the centre of the island for the time in (a); the dotted horizontal line in (a) and (c) marks the position of the centre of the island for the time in (c). These two lines show that the island hardly moves during the transition.

e.g. the line that starts at $I \simeq 70.8, \theta/2\pi = 0$ curves down to $I \simeq 70.0, \theta/2\pi \simeq 0.25$ etc. These are the trajectories where the electron is not locked to the phase of the microwave, but the microwave field perturbs the energy depending on the radial position of the electron. This region also gives stable, regular trajectories. Finally, there is a region of chaos that separates the three regions. This chaotic region has a large X-like character

near $I \simeq 74.5, \theta/2\pi \simeq 0.75$ but extends in a thin band that circles the island of stability.

The sequence of graphs is snapshots in time from just before (figure 8(a)), to during (figure 8(b)), to after (figure 8(c)) the transition. These graphs give a clear indication of the mechanism for giving a small range of final energies. At very early times, the field is weak and the frequency is strongly detuned so that the points on the phase space plot would be all on the line $I = 72$. As the field increases, an island of stability forms whose size increases with field strength and position depends on the condition that the Rydberg frequency matches the microwave frequency. Because of the chirp, the centre of the island moves to smaller I. Just before the transition (figure 8(a)), the trajectories lie on a simple curve that is just below the chaotic region. During the transition (figure 8(b)), the chirp brings the chaotic region into the phase space inhabited by the trajectories and the motion becomes chaotic. While the trajectories are in the chaotic region, the edge of the chaotic region is moving downwards in I. Thus, a trajectory is most likely to leave the chaotic region by getting into the regular part of phase space by leaving through the upper edge of the chaotic region. Just after the transition (figure 8(c)), the electrons are in the regular region again. If the chirp is not too large then they will tend to leave the chaotic region at similar positions of the edge. Thus, they tend to roughly lie on a single band as clearly seen in figure 8(c).

The sequence in figures 8 is for the field strength just large enough for transitions to occur. If the field is larger, then the spread in final energies becomes greater because the chaotic region is larger. The spread in final energies also increases if the size of the chirp increases because then the trajectories randomly leave the chaotic region for quite different values of I.

One of the interesting features of this interpretation is that the transition occurs through the chaotic region of phase space but yields a final product that is localized to a small energy region. Within the classical model, there is zero probability for a transition unless the size of the island gets large enough to reach the regions of the trajectory, and the states that it reaches depends on the width of the island. A final interesting feature is that we did not see transitions into the stable island; this is due to the fact that the region of phase space that is entering the chaotic region is at the upper edge of the small I regular region and the region of phase space that is leaving the chaotic region is at the lower edge of the large I regular region. All of these observations are in agreement with the general treatment of transitions through a separatrix [4, 5]. Reference [6] observed a similar effect for a driven Morse oscillator; however, in this work, they did not chirp the field and, thus, the transition probability to the upper state remained substantially less than 1. We also performed calculations with no chirp and found that we could get transitions to the correct energy but again with an efficiency reduced from 1 which shows that the chirp is useful for increasing the efficiency of the transition.

5. Conclusions

We have performed calculations of the multiphoton adiabatic rapid passage measured in [3]. As in [3], we observed multiphoton transitions using relatively small amount of the chirp. Although the transitions seemed to be simple, the angular momentum distribution in our wavefunction shows that the actual number of absorbed/emitted photons is roughly an order of magnitude more than that might be expected.

We also analysed the result of a classical calculation and found that transitions with a high degree of localization of the final energy can be obtained; we traced this to the jump of an adiabatic invariant due to a separatrix crossing. The fact that the transitions to well-defined final energies can occur because of the separatrix crossing is interesting in that it greatly differs from the usual method of moving population in phase space which relies on capturing the population in an island and moving the island adiabatically by changing a parameter in the Hamiltonian. As suggested in [3], we expect that these results can be applied to other nonlinear oscillators like molecular vibrations, molecular rotations, the kicked rotor and a kicked Rydberg electron. In addition to investigations of different anharmonic oscillators, it would be interesting to study the role of a chirp and the role of the time-dependent strength of the driving term. It would also be interesting to understand whether transitions through multiple separtrix crossings could lead to higher control of the final state compared to transitions through a single separatrix.

Acknowledgments

We are grateful for substantial discussions with T F Gallgher and J D Hanson. This work was supported by the Office of Fusion Energy Sciences, US Department of Energy.

References

[1] Maas D J, Duncan D I, Vrijen R B, van der Zande W J and Noordamm L D 1998 *Chem. Phys. Lett.* **290** 75
[2] Maeda H, Norum D V L and Gallagher T F 2005 *Science* **307** 1757
[3] Maeda H, Gurian J H, Norum D V L and Gallagher T F 2006 *Phys. Rev. Lett.* **96** 073002
[4] Tennyson J L, Cary J R and Escande D F 1986 *Phys. Rev. Lett.* **56** 2117
[5] Cary J R, Escande D F and Tennyson J L 1986 *Phys. Rev.* A **34** 4256
[6] Dietz K, Henkel J and Holthaus M 1992 *Phys. Rev.* A **45** 4960
[7] Topcu T and Robicheaux F 2007 *J. Phys. B: At. Mol. Opt. Phys.* **40** 1925